Journal of Hydrology 598 (2021) 126240

Contents lists available at ScienceDirect

Journal of Hydrology

journal homepage: www.elsevier.com/locate/jhydrol

Research papers

Excitation-emission matrix fluorescence spectra of chromophoric dissolved organic matter reflected the composition and origination of dissolved organic carbon in Lijiang River, Southwest China

Qiufang He [a,b], Qiong Xiao [b], Jiaxing Fan [a], Haijuan Zhao [a], Min Cao [a], Cheng Zhang [b], Yongjun Jiang [a,*]

[a] Chongqing Key Laboratory of Karst Environment & School of Geographical Sciences, Southwest University, Chongqing 400700, China
[b] Key Laboratory of Karst Dynamics, Ministry of Nature Resources/Guangxi, Institute of Karst Geology, Chinese Academy of Geological Sciences, Guilin 541004, China

ARTICLE INFO

This manuscript was handled by C. Corradini, Editor-in-Chief

Keywords:
CDOM
Microbes
Photosynthesis
EEM-PARAFRAC
Surface karst aquatic system

ABSTRACT

Aquatic photosynthesis transforms inorganic carbon to organic carbon (OC), which contributes to autochthonous organic carbon (AOC) in sediment and particulate organic carbon in surface karst aquatic systems. Aquatic plant and microbes are participated in autochthonous dissolved organic carbon (ADOC) formation in surface karst aquatic systems, but the composition and formation of ADOC remains little known, which leaves problem on calculation of organic carbon flux. In this study, the Lijiang River was chosen as typical surface karst river to identify the DOC composition and its origin, and to explore the environmental influencing factors. Samples were collected seasonally from the upper to lower reaches of the river to analyze hydrochemical parameters and the excitation-emission matrix (EEM) spectrum of chromophoric dissolved organic matter (CDOM). Three CDOM components were calculated by parallel factor analysis (PARAFAC) from EEM spectra, which were allochthonous soil-sourced DOC (SDOC), autochthonous aquatic plant-sourced DOC (APDOC), and microbial-sourced DOC (MDOC). Based on the DOC component concentrations, SDOC is induced by large amounts of precipitation causing soil erosion in summer. APDOC formation is encouraged by moderate water temperatures in spring and fall restricted by high water turbidity in summer. The significant positive linear correlations between APDOC and dissolved inorganic carbon (DIC) and MDOC indicate DIC fertilization effect in karst aquatic systems directly promotes APDOC formation and indirectly promotes MDOC. Our study develops a relatively simple way to calculate composition of karst aquatic DOC, which demonstrates the participation of aquatic plants and microbes in APDOC production and reiterate that autochthonous DOC should be considered when calculating the carbon sink in surface karst aquatic systems.

1. Introduction

The biological carbon pump (BCP) plays an important role in carbon cycling in karst surface freshwater ecosystem. It transforms inorganic carbon to autochthonous organic carbon (AOC), and contributes to a stable organic carbon (OC) sink (Liu et al., 2017, 2018a; Passow and Carlson, 2012; Yang et al., 2015). The BCP effect and aquatic photosynthetic formation of AOC have been observed via variations in hydrochemical and CO_2 emission in karst pools and reservoirs (Jiang et al., 2013; Pu et al., 2020; Zhang et al., 2017, 2019). Based on stable isotope fractionation and tracer modeling, high dissolved inorganic carbon (DIC) concentration promoted aquatic plant and phytoplankton photosynthesis production in karst aquatic systems, and photosynthetic AOC contributed 60–80% of total sediment and particulate OC in karst freshwater lakes and rivers in South China (He et al., 2020; Huang et al., 2020; Yang et al., 2016). Additionally, dissolved organic carbon (DOC) was observed to increase coupled with high concentration of DIC in karst aquatic systems (Kritzberg et al., 2006; Yuan, 2016), which accounted for more than 80% of the total OC in karst water. However, the effect and contribution of aquatic plant photosynthesis on the autochthonous DOC formation process remain unclear, which is adverse to calculating the carbon sink flux of autochthonous DOC in karst carbon cycling.

In addition, phototrophic bacteria were observed in karst aquatic systems, and engaged in the DIC-DOC transformation (Kolda et al.,

* Corresponding author.
E-mail address: jiangjyj@swu.edu.cn (Y. Jiang).

https://doi.org/10.1016/j.jhydrol.2021.126240
Received 23 December 2020; Received in revised form 16 March 2021; Accepted 18 March 2021
Available online 23 March 2021

2019; Li et al., 2018; Posth et al., 2017; Zhang et al., 2011), while heterotrophic bacteria were involved in the decomposition of autochthonous DOC produced by aquatic photosynthesis in karst aquatic systems (Kritzberg et al., 2006; Shabarova et al., 2014; Song et al., 2017). The participation of microbes produces microbial-sourced DOC (MDOC) production, which induces variation in DOC components and concentrations in karst aquatic system. Previous reports revealed that microbial-sourced organic matter was persistent and considered a more stable carbon sink in freshwater and marine systems (Jiao et al., 2010; Ogawa et al., 2001), but the characters of MDOC remain unclear in karst aquatic system. Also, the concentration and fraction of MDOC in karst aquatic system need more accurate assessment, thus MDOC flux and persistent organic carbon sink can be accurately calculated in karst aquatic system, which is the crucial link between aquatic photosynthesis and persistent organic carbon sink. However, the effective mothed that evaluates MDOC fraction is still in developing, and the environmental factors that influence MDOC formation remain unclear, which are antecedent conclusions before MDOC flux calculation.

Chromophoric dissolved organic matter (CDOM) is the optically measurable component of dissolved organic matter (DOM) in water. CDOM components and fluorescence indexes, calculated by excitation-emission matrix (EEM) spectroscopy coupled with parallel factor analysis (PARAFAC), were used to illustrate the dominant DOM composition, origin, and biochemical characteristics (Cooper et al., 2016; Moradi et al., 2018). The underground recharge from karst subterrane in surface estuaries had been distinguished by CDOM fluorescence index and components, which were characterized by low concentrations of OM, high protein-like fluorescence, and autochthonous and microbial origin (Arellano and Coble, 2015; Chen et al., 2010; Martínez–Pérez et al., 2019; Pain et al., 2020; Sakellariadou and Antivachis, 2018). The fluorescence index of cave dripping and spring water revealed autochthonous microbial origin and low humification. However, a humic-like component had also been detected, which indicated soil OC input (Birdwell and Engel, 2010; Hartland et al., 2010; Mudarra et al., 2011; Quiers et al., 2014; Simon et al., 2010; Tatár et al., 2004; Xie et al., 2008). In surface karst aquatic systems, including freshwater lakes, reservoirs, and rivers, CDOM components contained OC originating from terrestrial (soil), aquatic plant, and microbial organic matter (Cheng, 2014; Liu et al., 2018b; Lu, 2018). However, the temporospatial variation of CDOM components and concentrations in surface karst aquatic systems is seldom reported, which could be used to determine the origin and concentration of DOC components and influence factors and then calculate ADOC flux.

The Lijiang River, located in Guangxi, China, was selected as a typical example of a surface karst aquatic system to investigate autochthonous DOC formation and its influence factors in surface karst aquatic system. Water samples were collected from the upper to lower reaches seasonally to monitor the spatial and temporal variation in hydrochemistry and fluorescence spectrum characteristics. CDOM components were calculated from the EEM fluorescence matrix using a PARAFAC model. The ADOC and MDOC concentration were calculated basing on the CDOM component and DOC concentration. We supposed that the variation of CDOM spectrum characters could reveal the spatial and temporal variation of DOC components and the variation of DOC components would be influenced by aquatic plant and microbes. The spatiotemporal variation of ADOC and MDOC concentration can be used for calculation of refractory DOC flux in future work.

2. Method and materials

2.1. Study area

The Lijiang River is a typical karst river located in the upper reaches of the Guijiang River, which belongs to the Pearl River system, and originates from south of Laoshanjie Mountain, Guanxi Zhuang Autonomous Region, southwest China. The Lijiang River flows from north to south through a 12,690 km^2 watershed with a length of 164 km (Fig. 1). The Lijiang watershed mainly consists of: (1) a non-karst area in the upper reaches of L2 that is underlain by slightly metamorphosed Devonian granite; (2) a covered karst area in the middle reaches between sites L2 and L3 that is underlain by middle and lower Devonian red clasolite; and (3) a bare karst area in the downstream of L3 that is underlain by Triassic and Cretaceous carbonate rocks with a thickness of approximately 900–3000 m. As a percentage of the watershed, the non-karst area accounts for 51% of the total area, the covered karst area accounts for 7%, and the bare karst area accounts for 42% (Zhao, 2018).

Lijiang River watershed is significantly influenced by extreme humidity and high temperatures consistent with the Asian monsoon climate, with annual precipitation in the range of 1367–1932 mm. The discharge of the Lijiang River is closely correlated with precipitation. Precipitation in the wet season from March to August accounts for 80% of the precipitation for the whole year, while the dry season from September to February accounts for 20%. Consequently, the discharge of Lijiang River in the wet season is approximately 10 times that of the dry season. In 2017, the discharge at the L6 site was 606 $m^3 S^{-1}$ in July, 217 $m^3 S^{-1}$ in March, 84 $m^3 S^{-1}$ in September, and 52 $m^3 S^{-1}$ in December. The slope of the Lijiang River valley decreases from the upper to lower reaches, and is no more than 0.5% between sites L3 to L6. Thus, the river water between sites L3 and L6 flows slowly and maintains low turbidity unless storm events occur (Hu, 2016; Yuan, 2016; Zhao, 2018). At the upriver of Lijiang River, forest land covers 51.4% of the total area, which decreases to 14.2% in the mid- and down- stream (Yue and Chen, 2008). Heavy precipitation and anthropogenic activity are the main factor that induces soil erosion intensification and sediment yield increase in Lijiang River basin, which causes Lijiang River water becomes turbid and yellow in storm event (Chang, 2008; Yue and Chen, 2008; Zhang and Wang, 2016).

The annual average temperature in the Lijiang River watershed ranges from 16.5 to 20.0 °C, while the annual average duration of insolation is 1615 h per year. The duration of insolation is 1354 h when temperatures are higher than 10 °C, which accounts for 84% of the annual duration of insolation. The annual average number of non-frost days is 320 days per year. These features, combined with the Secchi disk depth of tens meters, allow for the growth of dense submerged aquatic vegetation in the riverbed. Although vegetation varies with respect to the geomorphic features of the river, dense submerged aquatic plants are observed in the Lijiang River, especially in the middle to lower reaches (between site L3 and L6). Typical native submerged C_3-macrophytes resulting from the surface waters of the South China Sea occur in the main channel, such as *vallisneria natans L.*, *potamogeton distinctus A. Benn.*, *ceratophyllum demersum L.* and *hydrilla verticillata*, representing 90% of the submerged aquatic vegetation (Wu and Bai, 2017). Other primary producers include a variety of filamentous benthic algae, as well as emergent and floating species that can become dominant in the channel margins.

2.2. Sampling

Six sampling sites were selected to monitor the hydrochemical parameters and CDOM fluorescence spectra in the Lijiang River, of which the locations are shown in Fig. 1. Sites L1 and L2 locate at non-karst and covered karst areas, respectively, while the other sites are located in the bare karst area. L3 locates at the urban area of Guilin city, L4 locates at the place most important turbidities import, L5 locates at the place major groundwater import and L6 locates at the end of Lijiang River which imports to Guijiang River about 20 km^2 later. In total, 24 water samples were collected in March, July, September, and December of 2017.

Duplicate 50 ml water samples were collected using brown glass bottles for DOC\CDOM and total organic carbon (TOC) concentration analysis, to which a 0.5 ml saturation $HgCl_2$ solution was added to avoid microbial degradation. The sample for DOC\CDOM analysis was filtered

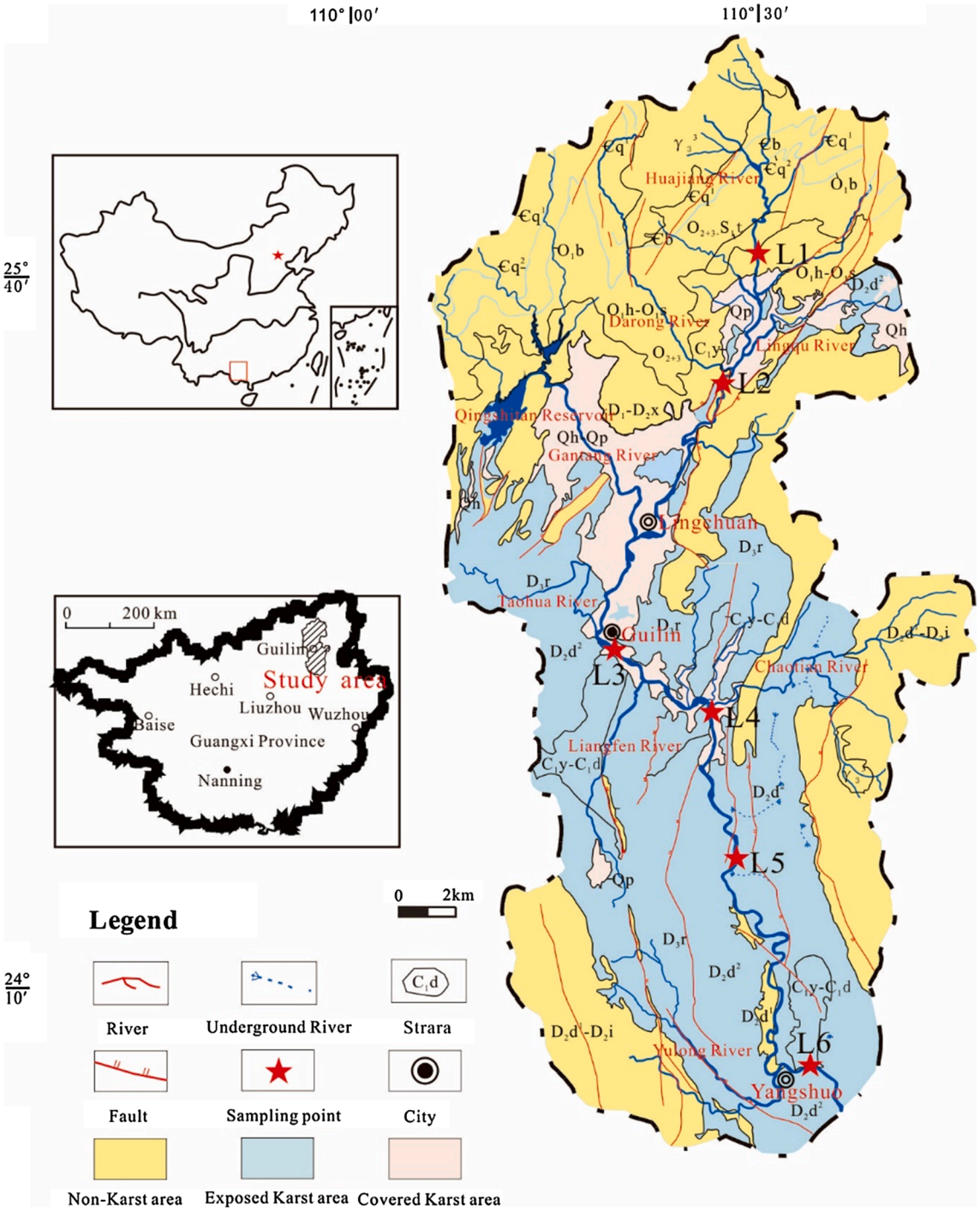

Fig. 1. Location and geological map of Lijiang River watershed (Modified from Zhao et al., 2018).

using a 0.70 μm fiberglass micro-membrane; the sample for TOC analysis was not subjected to this process. Glass bottles and fiberglass micro-membrane were heated at 300 °C for 3–4 h to remove all the organic matter before use. All sample bottles were rinsed 3–5 times using water sample before water samples were taken.

2.3. Hydrochemical analysis

A Manta Water-Quality Multiprobe (Eureka, USA) was used to determine the water temperature, pH, electronic conductivity (EC at 25 °C) (accuracy: 0.01 °C, 0.01 pH, 1 μS·cm^{-1}, respectively), as well as the concentration of dissolved oxygen (DO), total dissolved solid (TDS), turbidity (TUR), and chlorophyll *a* (Chl a) (accuracy: 0.1 μg L^{-1}). An alkaline testing kit (Merck, Germany) was used to determine the concentration of bicarbonate (HCO_3^-; 0.1 mmol L^{-1}). These parameters were measured in the field when the water samples were collected. Discharge data for the Lijiang River and its branches were obtained from the hydrological stations set by the Guilin Hydrographic Office (discharge and precipitation data used are given in the supplementary material).

Concentrations of TOC and DOC were analyzed by a Multi N/C 3100 analyzer (Analytik Jena AG, Germany, accuracy of 0.01 mg L^{-1}) in the Chongqing Key Laboratory of Karst Environment & School of Geographical Sciences, Southwest University, Chongqing, China. DOC

concentration of Gantangjiang River and three wells near L3 were monitored from March 2017 to January 2018 (the data were unpublished and got from Tao Zhang, Key Laboratory of Karst Dynamics, Ministry of Land and Resources/Guangxi, Institute of Karst Geology, Chinese Academy of Geological Sciences, Guilin, China).

2.4. EEM fluorescence analysis

The EEM fluorescence measurements were performed with a RF-5301PC spectrophotometer (Shimazu, Japan) equipped with a 150 W Xe lamp in the Chongqing Key Laboratory of Karst Environment & School of Geographical Sciences, Southwest University. EEM fluorescence spectrum matrices were obtained by emission scanning from 250 to 600 nm with 1 nm wavelength intervals at excitations from 220 to 500 nm and a 5 nm wavelength interval. A 1 cm × 1 cm × 4 cm quartz cuvette was used at room temperature (25 °C). Water Raman intensities were determined using deionized water (Millipore, USA) excited at 348 nm, with emissions monitored at 395 nm, which was consistently maintained during each session to guarantee equipment stability. The fluorescence emission intensity was normalized to the intensity of the lamp at the particular excitation wavelength applied (Zhang, et al., 2009). The fluorescence emission intensity was reported by QSU.

EEM matrices were analyzed using the PARAFAC multivariate modeling technique, which was performed in MATLAB (MathWorks, Natick, MA) with the DOMFluor toolbox (Stedmon et al., 2008). Raman and Rayleigh scattering were mitigated by subtracting the deionized water EEM spectrum collected from each corrected EEM and Delaunay triangular interpolation. Outlier samples were eliminated by checking component loadings and leverages of each sample. Split-half analysis and random initialization were used to validate the identified components (Stedmon et al., 2003). The maximum fluorescence intensity (FI) of each PARAFAC component (Fmax) and the percentages of each PARAFAC component in water samples was calculated (Korak et al., 2015; Osburn et al., 2013). The PARAFAC component position was determined by the component Fmax value and its Ex and Em wavelength. The PARAFAC component percentages and position were used to elucidate quantitative and qualitative variations in CDOM and DOM between water samples.

2.5. Organic matter concentrations

The concentration of CDOM was represented by the absorption at 355 nm. The CDOM absorbance spectra were obtained using a spectrophotometer (Shimadzu UV-2450PC UV–Vis spectrometer, Shimadzu Corporation, Kyoto, Japan) in a 1 cm × 1 cm × 4 cm quartz cuvette, recording absorbance values from 200 to 800 nm at 1 nm intervals. Pure water was used as blank (Milli-Q, USA). Average absorbance from 700 to 800 nm was subtracted from each spectrum to correct for offsets due to several instrument baseline effects (Helms et al., 2008). Absorbance measurements at each wavelength (λ) were baseline corrected by subtracting the absorbance at 700 nm. Absorption coefficients were obtained using the following equation (Zhang et al., 2009):

$$aCDOM(\lambda) = 2.303D(\lambda)/r \quad (1)$$

where aCDOM (λ) is the CDOM absorption coefficient at wavelength λ(nm), D (λ) is the corrected optical density at wavelength λ and r is the cuvette path length in m. In this study, the absorption coefficient at 355 nm (a355) was taken as a quantitative measure of CDOM. The linear fit of a355 absorbance and DOC concentration revealed significant correlation ($p < 0.001$, $R^2 = 0.95$, Fig. S1), which indicated CDOM cloud be used to invert the characters of DOC (Griffin et al., 2018). The linear fit of total fluorescence intensity (TF) and DOC concentration showed significant correlations ($p < 0.01$, $R^2 = 0.95$, Fig. S1), which indicated that the fluorescence intensity could be used to invert the characters of DOC.

The PARAFAC component position information was compared to published references to identify their biochemical characteristics (references were cites in 3.2), and these were used to distinguish the organic matter sources in this study.

The fluorescence of CDOM fluorophores fits concentration-fluorescence linear correlations, and the slope of linear relationship varies between individual PARAFAC components. Tryptophane and humic acid were measured as modal components to calculate the linear relationship of three PARAFAC components. The linear relationship functions were represented as following:

$$Ci = Si*FIi + Bi \quad (2)$$

Ci represented the concentration of model component i. FIi represented the fluorescence intensify of model component i, which was collected with fluorescence spectrometer from a series certain concentration solutions of model component i. Si was the slope of linear function and Bi was the intercept of linear function, which were calculated from linear fitting according to Ci and FIi. The concentration and fluorescence intensify data of model components were shown in Fig S2, as well as linear functions.

The concentration of three PARAFAC components were calculated according to the Eq. (2). FIi was the fluorescence intensify of individual PARAFAC component. The concentration of individual PARAFAC component could be calculated. The concentration of three organic carbon sources were calculated according to the percentage of individual PARAFAC component in DOC concentration.

2.6. Statistics

MATLAB 16.0 and DOMFluor toolbox were used to model the EEM PARAFAC analysis and calculate CDOM component factors. Origin 2018 was used to calculate the hydrochemical parameters and render the graphics. Linear regression was completed with Origin 2018 too.

3. Results

3.1. Hydrochemical characteristics

The hydrochemical parameters revealed different seasonal variations, in which water temperature, TUR, and TSM recorded the highest values in summer, whereas concentrations of Chl a recorded lower value in summer and winter (Fig. 2, Table S1). The water temperature in the Lijiang River was the highest in summer with the mean value of 26.0 °C, which followed by that in spring and fall with mean values of 15.5 °C and 19.2 °C, respectively, and lowest in winter with a mean value of 10.4 °C. The concentration of TUR and TSM were the highest in summer, of which the mean values are 14.9 mg L^{-1} and 15.9 mg/L, respectively. These were significantly higher than those in the other seasons, which ranged from 6.1 to 8.6 mg L^{-1} and 4.8–8.2 mg L^{-1}, respectively. Differently, the concentration of Chl a revealed higher value in spring and fall with the same mean value of 1.7 μg L^{-1}, but lower values in winter and summer with a man value of 0.7 μg L^{-1} and 0.8 μg L^{-1}, respectively.

The spatial variation of hydrochemical parameters exhibited a significant pattern of increasing concentrations from the upper to lower reaches, whereas TUR and TSM exhibited a decreasing pattern. The concentration of DIC increased from 3.8 to 13.9 mg L^{-1} at L1 to 35.1–58.0 mg L^{-1} at L6. The concentration of DOC increased from 1.1 to 1.8 mg L^{-1} at L1 to 2.6–4.1 mg L^{-1} at L6, of which the largest increase occurred between sites L2 and L3 (Fig. 2, Table S1). The concentration of TOC increased from 1.1 to 2.2 mg L^{-1} at L1 to 3.4–5.1 mg L^{-1} at L6, of which the largest increase occurred between sites L2 and L3. The box plot of DOC concentrations revealed that DOC in Gantangjiang River were significantly higher than that at L2, and the DOC in groundwater was 2.51 mg L^{-1} in average which was lower than that at L3 to L6 (Fig. 3).

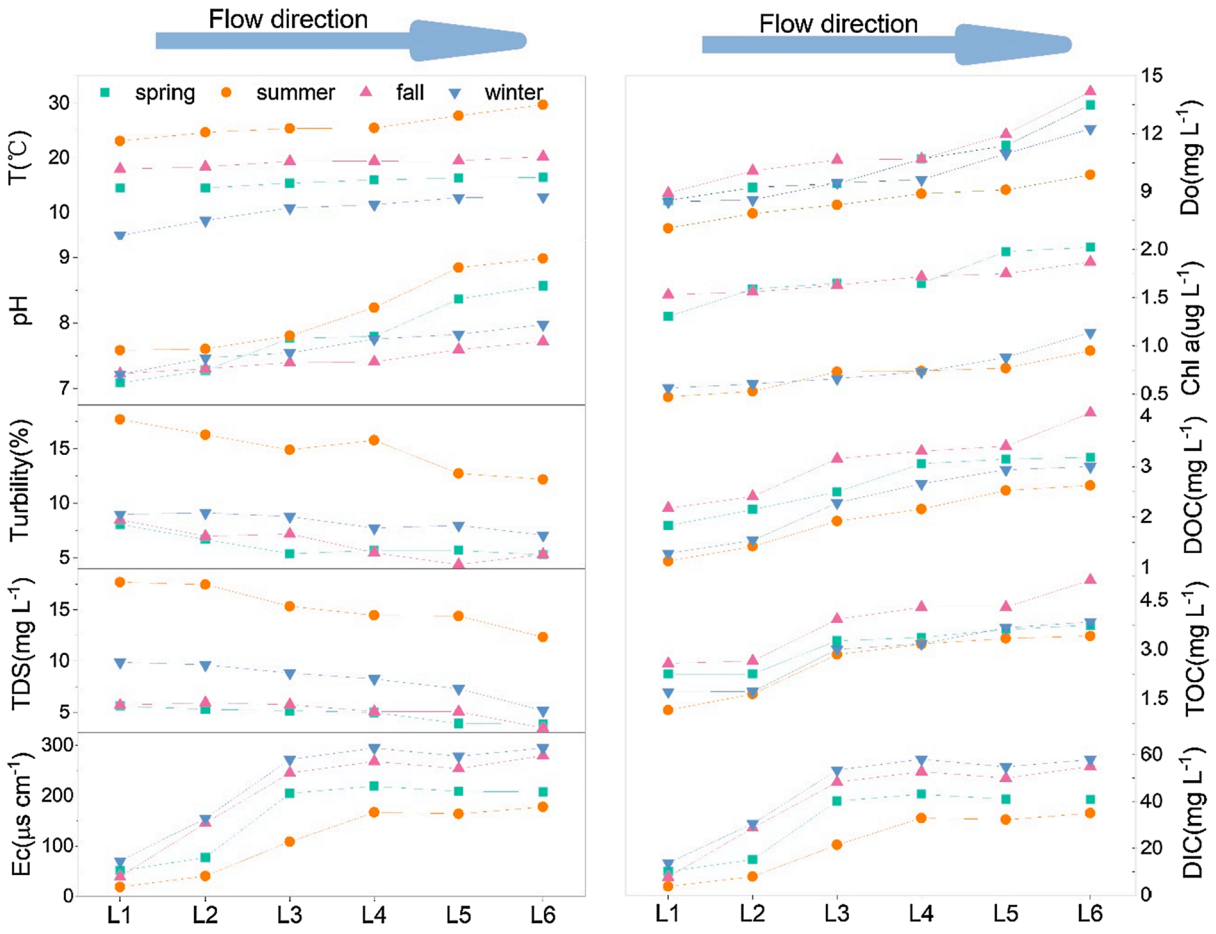

Fig. 2. Hydrochemical characteristics of the Lijiang River from the upper to lower reaches. Sampling sites L1 to L6 are also shown.

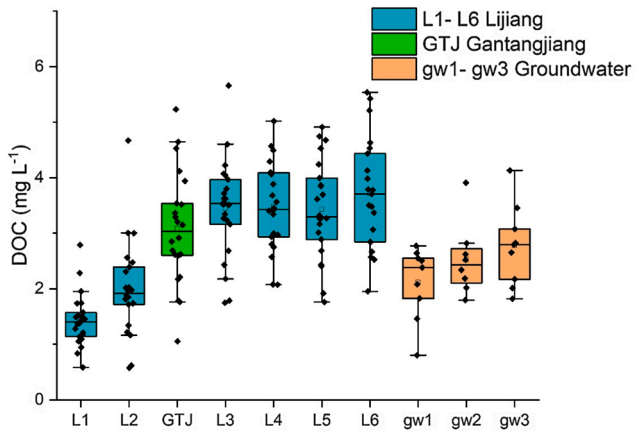

Fig. 3. DOC concentrations of Lijang River, Gantangjiang River and groundwater. L1–L6: sampling sites of Lijiang River; GTJ: Sampling site of Gantangjiang River, which represented the water from Qingshitan Reservoir; gw1-gw3: ground water sampling site near L3.

3.2. CDOM components

According to the PARAFAC modelling results, three fluorescence components were identified. These were two protein-like components (tryptophan) C1 ($\lambda_{ex}/\lambda_{em}$: 280/324 nm) and C3 ($\lambda_{ex}/\lambda_{em}$: ≤250/368 nm), and one humic-like component C2 ($\lambda_{ex}/\lambda_{em}$: 315/414 nm) (Fig. 4).

Component C1 is similar to peak T1 (T_1 = $\lambda_{ex}/\lambda_{em}$: 270–295/330–380 nm) which was found in uncontaminated aquatic systems and originated from phenolic and algae cellular substance decomposition (Martínez–Pérez et al., 2019; Murphy et al., 2006; Zhou et al., 2019). Additionally, component C1 is similar to the tryptophan fluorophore peak 5 ($\lambda_{ex}/\lambda_{em}$: 270–280/335–340 nm) in freshwater algae cultivation experiments on the phytoplankton bloom and cultivation period (Wang et al., 2012). Thus, in this study, component C1 is identified as an autochthonous organic matter component sourced from aquatic plant.

Component C2 is similar to peak C (C = λex/λem: 300–350/400–460 nm) which was found in uncontaminated aquatic systems (Garcia et al., 2015; Shutova et al., 2014; Zhou et al., 2019) and represents long wavelength humus. This component is also similar to the humic-like component peak 3 ($\lambda_{ex}/\lambda_{em}$: 310–330/420–455 nm) characterized as long-chain alkane and less aromatic carbohydrate, which originates from allochthonous decomposed soil organic matter (Cawley et al., 2012; Hambly et al., 2015; Wang et al., 2012). In this study, component C2 is identified as allochthonous soil sourced organic matter.

Component C3 is similar to peak T2 (C = λex/λem: 210–240/330–380 nm) which was found in uncontaminated aquatic systems and characterized as a tryptophan substance related to microbial involved decomposition (Mudarra et al., 2011). Component C3 is also similar to microbial related peak 4 ($\lambda_{ex}/\lambda_{em}$: 200–215/330–345 nm), of which the fluorescence intensity increases with increased microbial colony (Lee et al., 2018). Peak T2 was also reported to be an indicator of microbial decomposition in research on organic matter composition in urban-influenced and anthropogenic contaminated aquatic systems (Bricaud et al., 1981; Hong et al., 2005; Mudarra et al., 2011). In this study, component C3 is identified as autochthonous organic matter originating from microbes.

The total fluorescence intensities revealed a pattern of variation in CDOM concentrations. The total fluorescence intensity in spring and fall

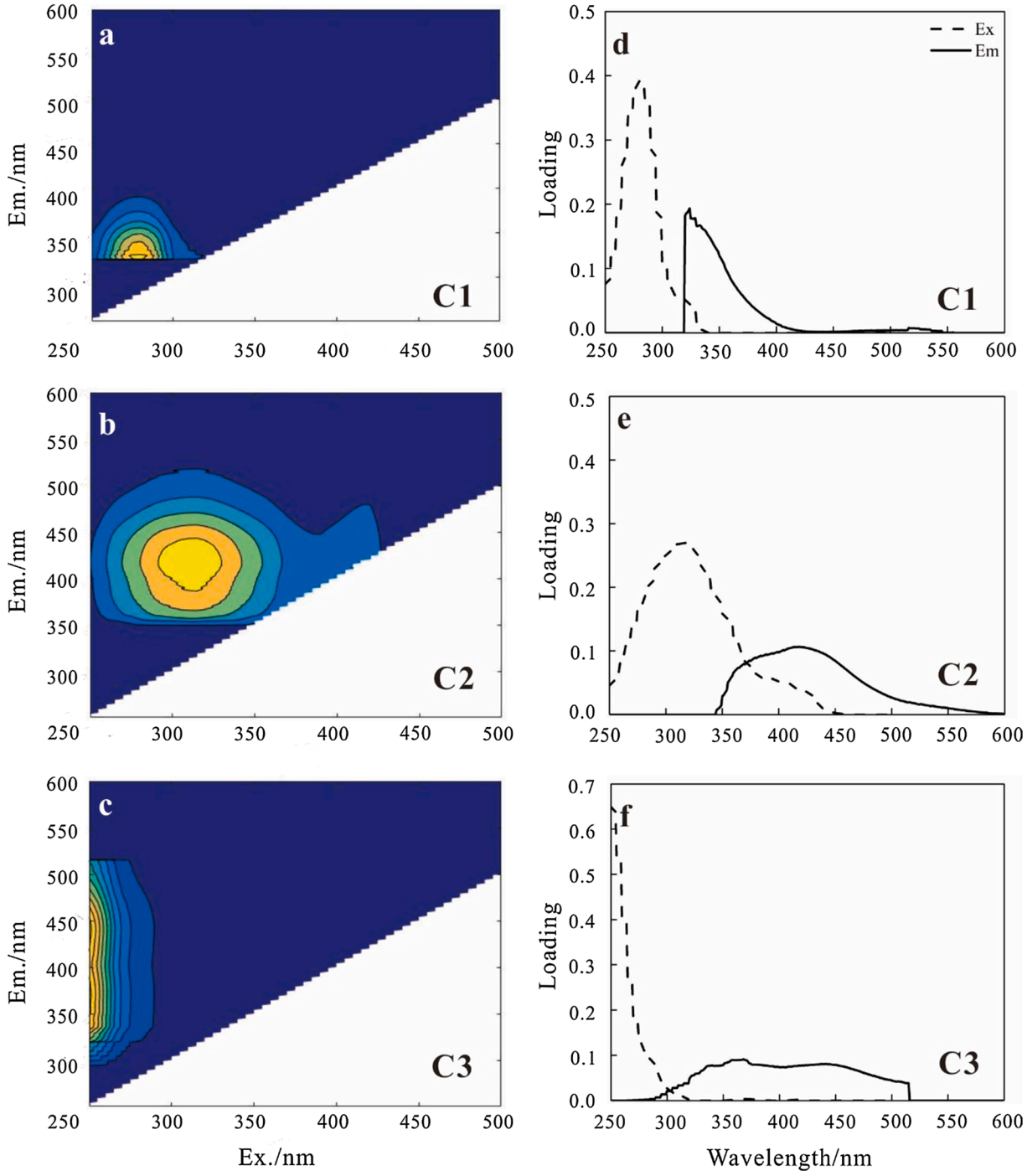

Fig. 4. EEM contours of the three fluorescent components identified by PARAFAC. a, d: intensify contour and split-half analysis of component C1; b, e: intensify contour and split-half analysis of component C2; c, f: intensify contour and split-half analysis of component C3.

ranged from 32.7 to 37.6 QSU with mean values of 35.2 and 36.3 QSU, respectively. The intensities in winter ranged from 25.7 to 30.0 QSU with a mean value of 27.8 QSU, while the lowest fluorescence intensities were recorded in summer, which ranged from 17.5 to 20.4 QSU with a mean value of 19.0 QSU (Fig. 5a).

Based on the percentages of the three components calculated from the fluorescence intensities, the fractions of components C1 and C3 showed an increase from the upper to lower reaches; however, the fraction of component C2 decreased (Fig. 5b). The fractions of component C1 increased from 19 to 32 % at L1 to 25–41% at L6, while the fractions of component C3 increased from 31 to 40 % at L1 to 40–42% at L6. In contrast, the fraction of component C2 declined from 33 to 50 % at L1 to 20–41% at L6. Because components C1 and C3 are autochthonous, the autochthonous DOC fractions increased from the upper to lower reaches and account for 59–80% in the lower reaches, which was the dominant component in Lijiang River.

3.3. Seasonal and spatial variation of DOC components

The concentrations of APDOC, allochthonous soil-sourced DOC (SDOC), and MDOC in each sample were calculated based on Eq. (2). As shown in Fig. 5a, the concentrations of APDOC and MDOC were higher

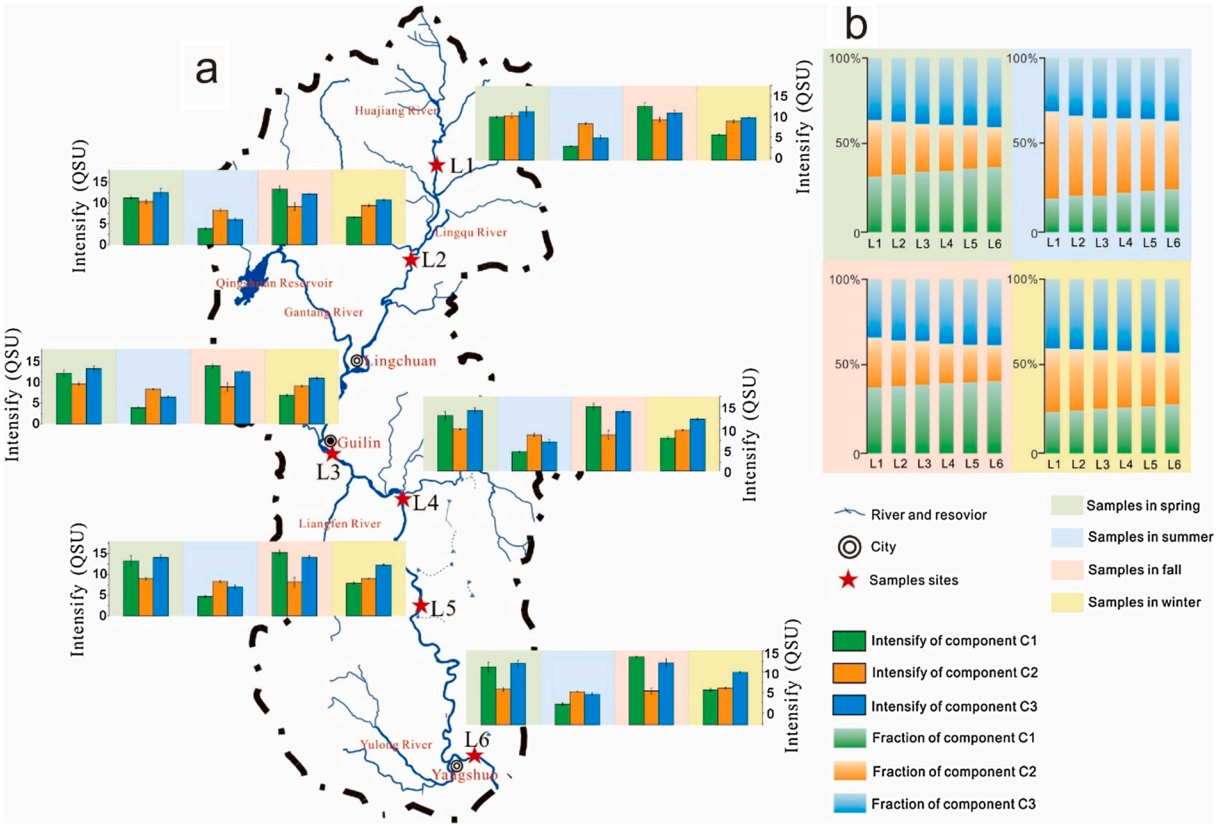

Fig. 5. Intensities and fractions of CDOM components in Lijiang River. a. Spatiotemporal variation of the three CDOM component intensities (quantified as QSU). b. Spatiotemporal variation of the three CDOM component fractions.

than those of SDOC in spring and fall, but lower than that of SDOC in summer. The three DOC components showed increase trend from the upper reach site L1 to the lower reach site L6, which indicated accumulation of organic matter in the aquatic system (Fig. 6).

As shown in Fig. 6b, the largest increases in the three types of DOC occur between sites L2 and L3, where the increases are 0.29 ± 0.10 mg L^{-1} for APDOC, 0.09 ± 0.06 mg $L^{-1}$for SDOC, and 0.16 ± 0.05 mg L^{-1} for MDOC. The largest increase between sites L2 and L3 indicated that a considerable quantity of organic matter, including from the three sources, recharged the Lijiang River in the upper reaches above L3. Besides the increases between sites L2 and L3, APDOC and MDOC increase significantly along the path of the river, whereas SDOC undergoes relatively stable recharge in the Lijiang River. The increases in DOC concentrations between other adjacent sampling sites were much less than those between L2 and L3, with APDOC ranging from 0.07 to 0.43 mg L^{-1}, MDOC ranging from 0.06 to 0.17 mg L^{-1}, and SDOC ranging from 0.01 to 0.10 mg L^{-1}.

4. Discussion

4.1. Ground discharge of OC to Lijiang River

Lijiang River develops in peak forest karst plain at Guiling, Guangxi, China. Although there are plenty of groundwater recharges to surface river in most of the karst area, only a few of subsurface river is found recharging to Lijiang River in Lijiang catchment. As show in Fig. 1, the main subsurface rivers are found between site L3 to site L6. The biggest groundwater is Guanyan River which recharges to Lijiang River near sampling site L5, and some small springs recharge to Lijiang River at riverbed. To investigate the influence of groundwater, the OC concentration and discharge between site L3 and L6 were detected to calculate the DOC flux. Discharge data were shown in Table 1, including three big turbidities Yulong River, Liangfeng River and Chaotian River and Lijiang River main stream. Data were collected in July, October 2017 and January 2018. Groundwater DOC concentration was shown in Fig. 3, of which three wells near L3 were collected from March 2017 to January 2018. The discharge of groundwater was calculated by the increment discharge from L3 to L6 subtracting the total discharge of three major turbidities. The DOC concentration of groundwater was represented by the mean DOC concentration of three wells in the same month. DOC flux was calculated by the DOC concentration multiplied discharge. The data in Table 1 showed that DOC flux of groundwater were 301.0 g S^{-1}, 28.7 g S^{-1} and 23.0 g S^{-1}, which accounted for 24%-36% of the DOC flux increment from site L3 to L6 and 11%- 13% of the total DOC flux at L6. The proportions of groundwater DOC flux indicated that groundwater was not the dominant organic matter recharge source of Lijiang River. The DOC recharge from surface turbidity and autochthonous OC should be the dominant DOC source of Lijiang River.

4.2. Temporal factors influencing OC concentrations

APDOC and MDOC showed significantly higher concentrations in spring and fall than in summer; however, SDOC revealed an inverse seasonal variation. The seasonal variation indicated that DOC components were influenced by different environmental factors.

The SDOC showed remarkable increases in summer that correlated with discharge, TUR, and TSM, each of which is influenced by precipitation. The higher concentrations of TUR and TSM indicated higher quantities of particulate matter and turbulence, which were induced by high flow velocity in the Lijiang River and soil erosion in the watershed (Wang, 2013). In summer, the precipitation was 910 mm and accounted for 49% of the annual precipitation, such that the discharge at site L6 was 606 L/S in July, which was 2.8–11.4 times of that in the other seasons. The heavy and frequent storm events resulted in intensive soil

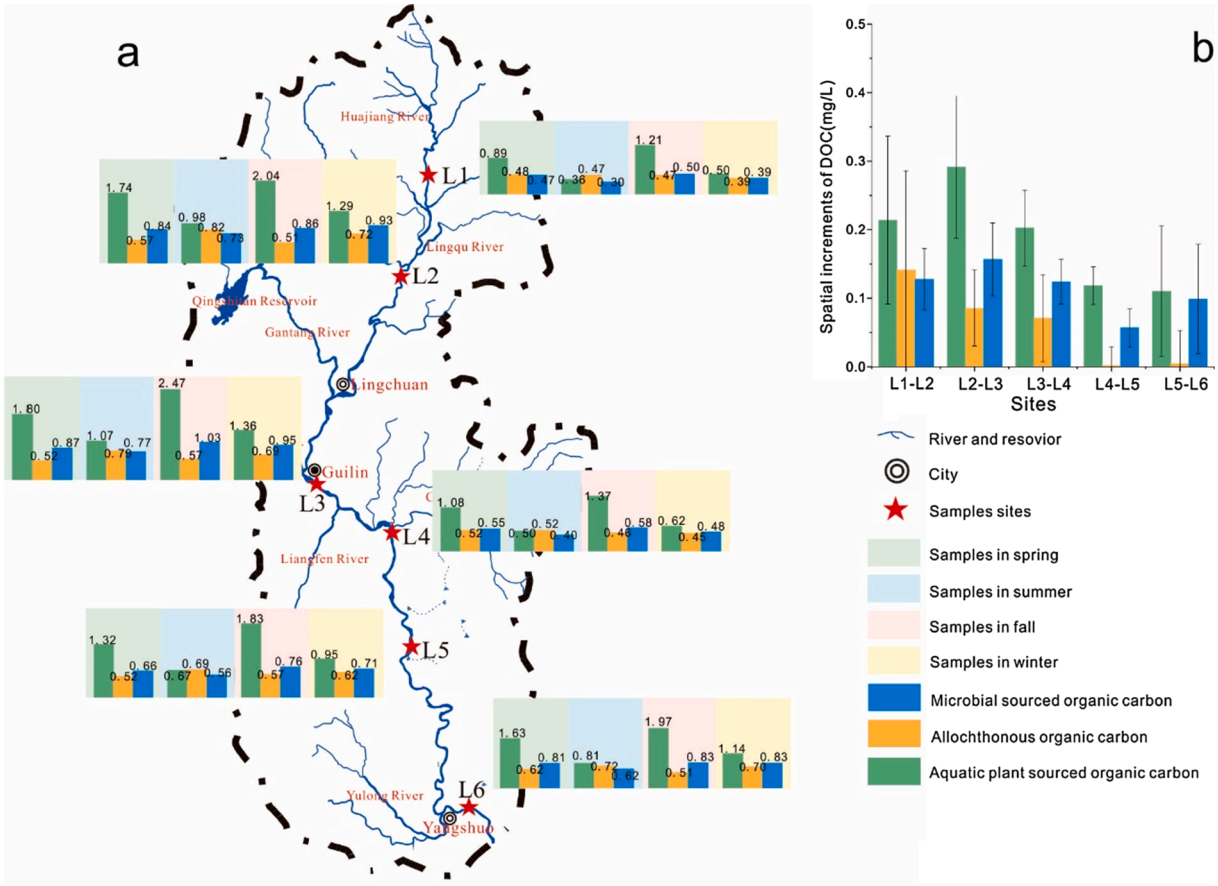

Fig. 6. The spatiotemporal variation of organic carbon (OC) components in the Lijiang River. a. Spatiotemporal variation of OC concentrations from allochthonous, microbes and aquatic plant sources (quantified as mg L^{-1}). b. Increment of OC component concentration between adjacent sampling points.

Table 1
DOC flux calculation of Lijiang River catchment.

Sites	Discharge (m^3 S^{-1})			DOC (mg L^{-1})			DOC Flux (g S^{-1})			
	Jul	Oct	Jan	Jul	Oct	Jan	Jul	Oct	Jan	
Turbidity	Yulong River	37.7	1.5	2.1	3.23	5.10	3.41	121.8	7.7	7.2
	Chaotian River	38.1	9.5	6.3	2.70	2.09	3.16	102.9	19.9	19.9
	Liangfeng River	158.7	6.4	5.1	3.82	5.32	4.65	606.2	34.1	23.7
	Total	234.5	17.4	13.5				830.9	61.6	50.8
Main stream	L3	442	55.8	37.5	3.15	2.53	2.94	1392.3	141.2	110.3
	L6	827	83.5	58.5	3.19	2.63	3.00	2638.1	219.6	175.5
	Increment	385	27.7	21				1245.8	78.4	65.3
	Groundwater	150.5	10.3	7.5	2.00	2.79	3.07	301.0	28.7	23.0

erosion in the watershed and high discharge flow velocities of the Lijiang River, which also consequently induced increase TUR, TSM, and soil-sourced organic matter (Wang, 2013). As shown in Fig. 6a, the average concentration of SDOC was 0.67 mg L^{-1} in summer, which was 113–130% of that in spring, fall, and winter (Fig. 7a). The concentrations of SDOC revealed significant positive correlations with that of TUR (Fig. 7b. $R^2 = 0.84$, $p < 0.05$). Thus, precipitation is the main factor causing seasonal variation in allochthonous SDOC.

The highest concentrations of APDOC were recorded in fall, while the lowest concentration was recorded in summer. Chl a concentration exhibited similar seasonal variation. The concentrations of Chl a and APDOC were observed to have a very strong correlation (Fig. 7d: $R^2 = 0.95$, $p < 0.01$). The concentration of Chl a is an important indicator of primary productivity that indicates the quantities of pigment and planktonic algae in aquatic systems (Sasaki et al., 2005). The significant correlations with APDOC indicate that aquatic plant photosynthesis is the main source of APDOC, and that the environmental factors that influence aquatic plant photosynthesis would be the main factors influencing the concentrations of APDOC.

The temperature and turbidity of the Lijiang River are influenced by the Asian monsoon, which impacts aquatic plant photosynthesis, and consequently, induces seasonal variation in APDOC. Aquatic plants in the Lijiang River are heliophile and thermophile, which grow well in aquatic systems with the water temperature ranges from 15 to 30 °C (Li, 2007). Thus, the aquatic plants grow well in spring, summer, and fall when the average water temperatures are 19.2, 26.0, and 15.5 °C, respectively; however, they exhibit restricted growth in winter when the average water temperature is 10.4 °C (Fig. 7c). In addition, the water turbidity in summer increased significantly, which induced insufficient illumination in the river water, and consequently restricted aquatic plant photosynthesis. Thus, APDOC was observed at lower concentrations in winter and summer, due to low temperatures and high turbidity,

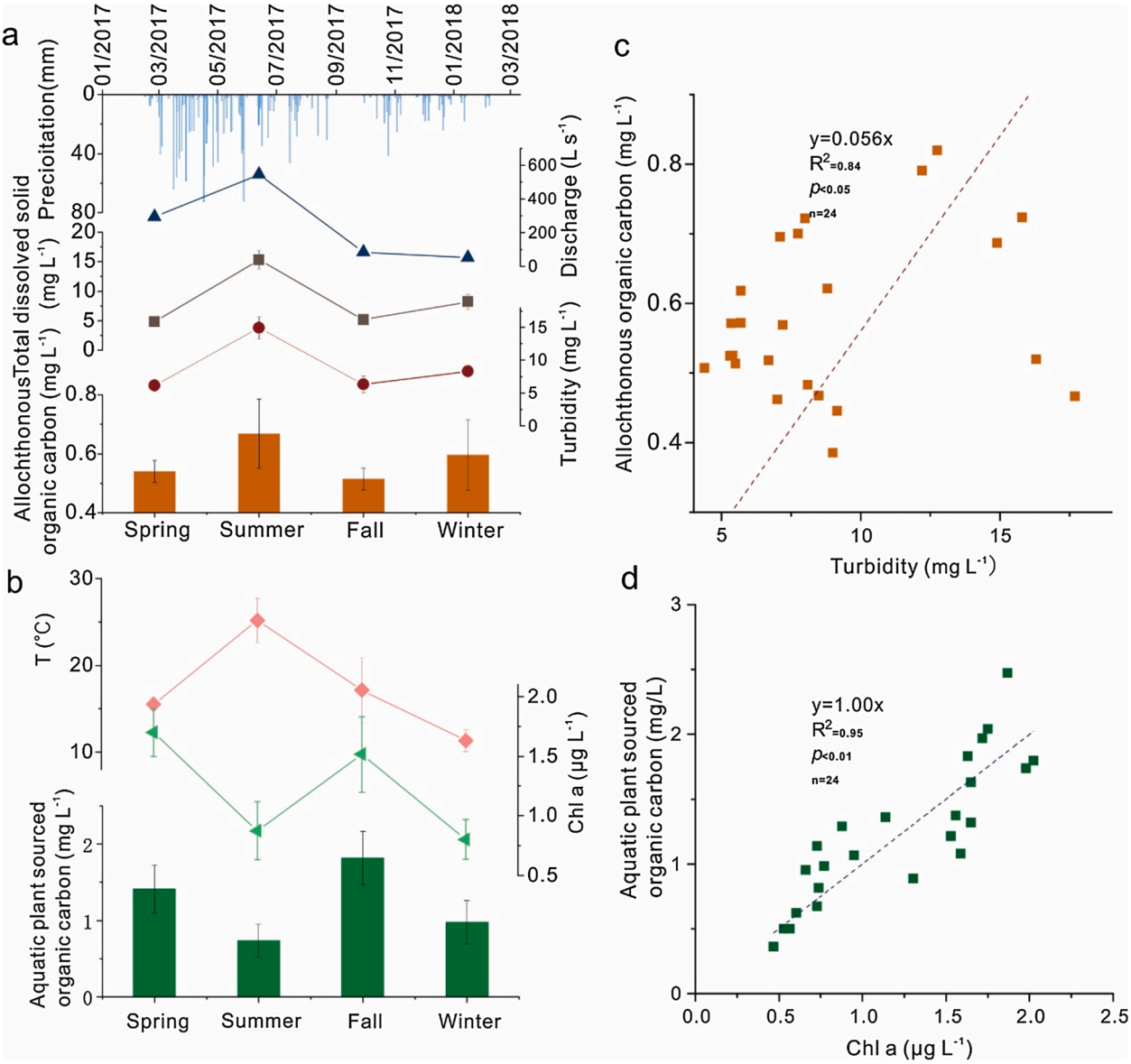

Fig. 7. Seasonal variation of APDOC and allochthonous organic carbon (AOC) and their influence factors. a. Seasonal variation of AOC, TSM, TUR, and discharge and precipitation. b. Linear regression of TUR and AOC concentrations. c. Seasonal variation of APDOC, Chl a, and temperature. d. Linear regression of Chl a and APDOC concentrations.

respectively, restricting aquatic plant photosynthesis and growth.

4.3. Spatial factors influencing OC concentrations

The concentrations of DIC in the lower reaches (from sites L3 to L6) ranged from 21.5 to 58.0 mg L^{-1}, which is 2.3–7.5 times of that at L1 (Fig. 2). According to previous reports, Lijiang River is significantly recharged from allochthonous water which is corrosive to carbonate bedrock. As Zhao et al. (2020) and Sun et al. (2019) reported, DIC was dominantly originated from carbonated weathering but not organic matter. The high concentrations of DIC in the karst area promoted aquatic plant photosynthesis (Liu et al., 2018a; Yang et al., 2015), which induced significantly increased concentrations of Chl a, the indicator of photosynthesis, in the downstream karst area. Thus, the concentrations of Chl a were shown to have a similar increasing pattern, insofar as the increase between sites L3 and L6 ranged from 0.31 to 0.54 mg L^{-1}, which was 1.5–13.4 times that between sites L1 and L2 (Fig. 2). On the other hand, plenty of N and P input could result in phytoplankton increase, large-scale submerged plant inhabitation and DOC increase in aquatic system. As shown in Table S1, the major cation and anion concentrations revealed that water samples of Lijiang River contained very low concentrations of inorganic nutrients. Lijiang River has good water quality, in which large-scale submerged plant is the dominant aquatic species and the main nutrient source is sediment or soil at riverbed. And the limited nutrient of plant in karst area is C but not N and P, thus, the DIC fertilization is the main reason of DOC formation. Consequently, APDOC, the product of aquatic plant photosynthesis, was observed to have increased significantly, while the concentrations revealed a significant linear correlation with DIC concentrations in the Lijiang River (Fig. 8; $R^2 = 0.88$, $p < 0.01$). The concentration of APDOC and MDOC revealed significantly positive correlations with DIC, which indicates that DIC fertilization effect was an important factor promoting increases in autochthonous DOC.

The microbial community in surface freshwater is dominated by heterotrophic species which need organic matter as an energy and carbon source (Shabarova et al., 2014). Allochthonous organic matter has a high humification organic component, and the heterotrophic species thus decompose small molecular labile organic matter produced by

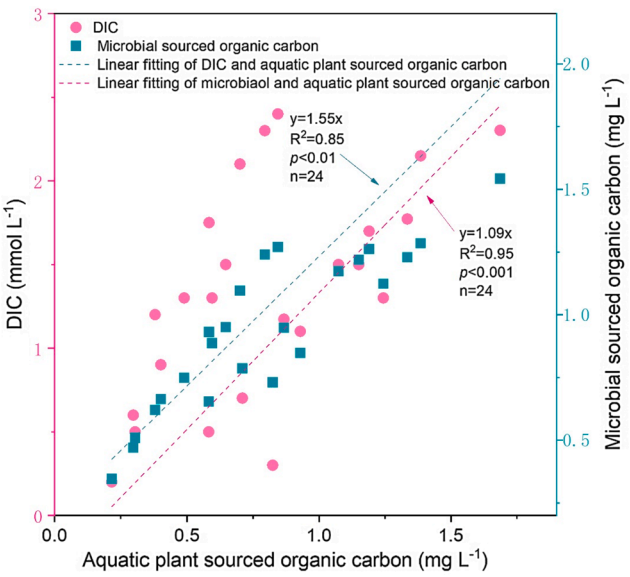

Fig. 8. Linear regression of APDOC-DIC and APDOC-MDOC.

aquatic plants as a carbon and energy source (Kritzberg et al., 2006; Obernosterer and Benner, 2004; Zhang et al., 2009). The concentration of MDOC is influenced by the abundance of APDOC, and their concentrations reveal a significant linear correlation (Fig. 8; $R^2 = 0.94$, $p < 0.001$). Progressively increasing DIC concentrations were observed from the upper to lower reaches of the Lijiang River, which promoted the increase in APDOC, and consequently, induced an increase in MDOC.

As reported by Huang et al. (2020) and Pu et al. (2020), reservoirs are also important inorganic and OC sinks in karst areas. Thus, the Gantangjiang River, which has its source from the Qingshitan Reservoir and recharges to the Lijiang River in the upper reaches at L3, is an important OC recharge source of the Lijiang River. The Qingshitan Reservoir is located in the upper reaches of the Gantangjiang River, two thirds of the area of which is distributed in bare karst areas (Fig. 1). The DOC and DIC concentration of Gantangjiang River were significantly higher than that in L2 (Fig S2 and Table S1). According to the discharge data from the Guilin Hydrological Station, the discharge of the Gantangjiang River was 19, 48, 21, and 14 $m^3 \cdot s^{-1}$, in spring, summer, fall and winter, respectively, and corresponds to the largest recharge tributary of the Lijiang River. Thus, the water from the Qingshitan Reservoir contained high concentrations of DIC and DOC to recharge the Gantangjiang River, which induced impressive increases in DIC and DOC concentrations between sites L2 and L3.

According to the hydrological data in July 2017, October 2017 and January 2018, the flux of three organic sources were calculated (Table 2). Discharge data of July 2017 represented summer, of which October 2017 represented fall and January 2018 represented winter. The autochthonous DOC flux from L3 to L6 were 1075.9 g S^{-1} in summer, 130.2 g S^{-1} in fall and 59.0 g S^{-1} in winter, which accounted for 79% − 87% of the total DOC flux increment. Significant variation had been found in different season for the river discharge changed. Thus, in the future work, more frequently sampling and monitoring should be applied based on the temperature and hydrological condition variation to investigate the precise variation of APDOC and MDOC concentration in Lijiang river. Also, more sampling sites, including important turbidity import sites and groundwater, should be selected and monitored to calculate the exactly increment of autochthonous APDOC and MDOC in the surface karst aquatic system. According to the high frequency monitoring CDOM and hydrological data, the autochthonous APDOC and MDOC flux would be calculated accurately, which offers a simple and effective mothed to evaluated the organic carbon sink and DIC-DOC conversion rate in karst aquatic system.

5. Conclusions

Three CDOM components were detected in the Lijiang River, with Em/Ex wavelengths similar to those reported for CDOM peaks of soil-, aquatic plant- and microbial-sourced organic matter. The CDOM compositions and origins demonstrated that aquatic plants and microbes were involved in autochthonous DOC formation. The seasonal variation in OC compounds is linked to hydrochemical factors, including Chl a, TUR, TSM, and T, of which TUR and TSM were significantly influenced by the heavy precipitation in summer and Chl a was influenced by the aquatic plant growth in high temperature. Thus, precipitation and temperature are the most important environmental factors inducing increases of SDOC in summer and of APDOC in spring and fall. The spatial variation of APDOC and MDOC is linked to DIC, which indicates that the “DIC fertilization effect” promotes a pattern of increases in APDOC from the upper to lower reaches, which consequently induces increases in MDOC.

The results of this study offer evidence that microbes participate in DIC-DOC transformation and are indirectly influenced by the “DIC fertilization effect” and photosynthesis in karst systems. The APDOC and MDOC are important parts of the OC sink in karst aquatic systems, and need to be considered in karst aquatic carbon sink calculations. Also, a relatively simple mothed was developed to calculate DOC component concentration from CDOM EEM fluorescence spectrum, which offered effective and convenient way to determine the ADOC component and concentration.

CRediT authorship contribution statement

Qiufang He: Conceptualization, Visualization, Methodology, Writing - original draft, Writing - review & editing. **Qiong Xiao:** Writing - review & editing, Investigation. **Jiaxing Fan:** Methodology, Investigation, Visualization. **Haijuan Zhao:** Investigation. **Min Cao:** Writing - review & editing, Visualization. **Cheng Zhang:** Supervision, Funding acquisition. **Yongjun Jiang:** Supervision, Funding acquisition, Writing - review & editing.

Table 2
DOC flux of three organic sources.

		DOC concentration (mg L^{-1})			Discharge (m3 S^{-1})	DOC flux (g S^{-1})		
		APDOC	SDOC	MDOC		APDOC	SDOC	MDOC
Summer	L3	0.98	0.82	0.73	442	434.3	362.4	321.6
	L6	1.07	0.79	0.77	827	884.9	653.9	946.8
	Increment	0.08	−0.03	0.04	385	450.6	291.5	625.2
Fall	L3	2.04	0.51	0.86	55.8	113.9	28.3	48.1
	L6	2.47	0.57	1.03	83.5	206.3	47.7	85.9
	Increment	0.43	0.06	0.17	27.7	92.5	19.4	37.7
Spring	L3	1.74	0.57	0.84	37.5	65.2	21.5	31.5
	L6	1.80	0.52	0.87	58.5	105.0	30.7	50.7
	Increment	0.06	−0.05	0.03	21	39.8	9.2	19.2

Declaration of Competing Interest

The authors declare that they have no known competing financial interests or personal relationships that could have appeared to influence the work reported in this paper.

Acknowledgements

We thank the support of Guilin Hydrological Monitoring Station and Tao Zhang from Key Laboratory of Karst Dynamics, Ministry of Land and Resources/Guangxi, Institute of Karst Geology, Chinese Academy of Geological Sciences. They shared the data of main stream and tributaries discharge and DOC concentration of groundwater in Lijiang River catchment. This research was supported by the National Key Research and Developmental Program of China (2016YFC0502306), the Chongqing Municipal Science and Technology Commission Fellowship Fund (CSTC2019yszx-jcyjX0002), the Karst Dynamics Laboratory, MNR and GZAR (KDL&Guangxi 202007), International Partnership Program of Chinese Academy of Sciences (132852KYSB20170029-01), and the Guangxi Natural Science Foundation (2018GXNSFDA05000), Global Karst Resource Ecology United laboratory-Comparative study of classical karst areas between China and Slovenia (KY201802009).

Appendix A. Supplementary data

Supplementary data to this article can be found online at https://doi.org/10.1016/j.jhydrol.2021.126240.

References

Arellano, A.R., Coble, P.G., 2015. Assessing carbon and nutrient inputs in a spring-fed estuary using fluorescence spectroscopy and discriminatory classification. Limnol. Oceanogr. 60 (3), 789–804. https://doi.org/10.1002/lno.10078.

Birdwell, J.E., Engel, A.S., 2010. Characterization of dissolved organic matter in cave and spring waters using UV–Vis absorbance and fluorescence spectroscopy. Org. Geochem. 41 (3), 270–280. https://doi.org/10.1016/j.orggeochem.2009.11.002.

Bricaud, A., Morel, A., Prieur, L., 1981. Absorption by dissolved organic matter of the sea (Yellow Substance) in the UV and Visible CDOM. Limnol. Oceanogr. 26 (1), 43–53. https://doi.org/10.4319/lo.1981.26.1.0043.

Cawley, K.M., Ding, Y., Fourqurean, J., et al., 2012. Characterizing the sources and fate of dissolved organic matter in Shark Bay, Australia: a preliminary study using optical properties and stable carbon isotopes. Mar. Freshw. Res. 63, 1098–1107.

Chang, Y., 2008. The mechanism of overland flow yield in peak-cluster depression of southern China – a Case from the Guilin Karst experimental Site. Master Thesis. China University of Geoscience, Wuhan, China.

Cheng, Q., 2014, Sources and Characterization of organic carbon and nitrogen in plateau lake sediments:Taking Dianchi Lake for Example. PhD Thesis, East China Normal University, Shanghai, China.

Cooper, K.J., Whitaker, F.F., Anesio, A.M., Naish, M., Reynolds, D.M., Evans, E.L., 2016. Dissolved organic carbon transformations and microbial community response to variations in recharge waters in a shallow carbonate aquifer. Biogeochem. 129 (1-2), 215–234. https://doi.org/10.1007/s10533-016-0226-4.

Kritzberg, E.S., Cole, J.J., Pace, M.M., Granéli, W., 2006. Bacterial growth on allochthonous Carbon in humic and nutrient-enriched lakes: Results from whole-lake ^{13}C addition experiments. Ecosys. 9 (3), 489–499. https://doi.org/10.1007/s10021-005-0115-5.

Garcia, R.D., Reissig, M., Queimaliños, C.P., Garcia, P.E., Dieguez, M.C., 2015. Climate driven terrestrial inputs in ultraoligotrophic mountain streams of Andean Patagonia revealed through chromophoric and fluorescent dissolved organic matter. Sci. Total Environ. 521-522, 280–292. https://doi.org/10.1016/j.scitotenv.2015.03.102.

Griffin, C.G., Finlay, J.C., Brezonik, P.L., Olmanson, L., Hozalski, R.M., 2018. Limitations on using CDOM as a proxy for DOC in temperate lakes. Water Res. 144, 719–727. https://doi.org/10.1016/j.watres.2018.08.007.

Hambly, A.C., Arvin, E., Pedersen, L.-F., Pedersen, P.B., Seredyńska-Sobecka, B., Stedmon, C.A., 2015. Characterising organic matter in recirculating aquaculture systems with fluorescence EEM spectroscopy. Water Res. 83, 112–120. https://doi.org/10.1016/j.watres.2015.06.037.

Hartland, A., Fairchild, I.J., Lead, J.R., Baker, A., 2010. Fluorescent properties of organic carbon in cave drip waters: Effects of filtration, temperature and pH. Sci. Total Environ. 408 (23), 5940–5950. https://doi.org/10.1016/j.scitotenv.2010.08.040.

He, H., Liu, Z., Chen, C., Wei, Y.u., Bao, Q., Sun, H., Yan, H., 2020. The sensitivity of the carbon sink by coupled carbonate weathering to climate and land-use changes: Sediment records of the biological carbon pump effect in Fuxian Lake, Yunnan, China, during the past century. Sci. Total Environ. 720, 137539. https://doi.org/10.1016/j.scitotenv.2020.137539.

Helms, J.R., Stubbins, A., Rithchie, J.D., Minor, E.C., Kieber, D.J., Mopper, K., 2008. Absorption spectral slopes and slope ratios as indicators of molecular weight, source, and photobleaching of chromophoric dissolved organic matter. Limno. Oceanogr. 53 (3), 955–969. https://doi.org/10.4319/lo.2008.53.3.0955.

Hong, H., Wu, J., Shang, S., Hu, C., 2005. Absorption and fluorescence of chromophoric dissolved organic matter in the Pearl River Estuary. South China. Mar. Chem. 97 (1-2), 78–89. https://doi.org/10.1016/j.marchem.2005.01.008.

Hu, J., 2016. Research on land use changes and ecological effects in Lijiang River basin. PhD Thesis. Huazhong Agricultural University, Wuhan, China.

Huang, S., Pu, J., Li, J., Zhang, T., Cao, J., Pan, M., 2020. Sources, variations, and flux of settling particulate organic matter in a subtropical karst reservoir in Southwest China. J. Hydrol. 586, 124882. https://doi.org/10.1016/j.jhydrol.2020.124882.

Jiang, J., Hu, Y., Schirmer, M., 2013. Biogeochemical controls on daily cycling of hydrochemistry and d13C of dissolved inorganic carbon in a karst spring-fed pool. J. Hydrol. 478, 157–168. https://doi.org/10.1016/j.jhydrol.2012.12.001.

Jiao, N., Herndl, G.J., Hansell, D.A., Benner, R., Kattner, G., Wilhelm, S.W., Kirchman, D. L., Weinbauer, M.G., Luo, T., Chen, F., Azam, F., 2010. Microbial production of recalcitrant dissolved organic matter: Long-term carbon storage in the global ocean. Nat. Rev. Microbiol. 8 (8), 593–599. https://doi.org/10.1038/nrmicro2386.

Kolda, A., Petrić, I., Mucko, M., et al., 2019. How environment selects: Resilience and survival of microbial mat community within intermittent karst spring Krčić (Croatia). Ecohydrology 12 (2), e2063. https://doi.org/10.1002/eco.2063.

Korak, J.A., Rosario-Ortiz, F.L., Summers, S.R., 2015. Evaluation of optical surrogates for the characterization of DOM removal by coagulation. Environ. Sci.: Water Res. Technol. 1, 493–506. https://doi.org/10.1016/j.watres.2019.115321.

Lee, M.H., Osburn, C.L., Shin, K.H., et al., 2018. New insight into the applicability of spectroscopic indices for dissolved organic matter (CDOM) source discrimination in aquatic systems affected by biogeochemical processes. Water Res. 14(7):164–176 https://doi.org/10.1016/j.watres.2018.09.048.

Li, Q., 2007, Influence mechanism of environment factors on the growth and development of submerged macrophytes. PhD thesis. Nanjing Normal University, Nanjing, China.

Li, Q., Huang, Y., He, X., et al., 2018. The Concentration of recalcitrant dissolved organic carbon in the karst hydrosphere and their existing mechanism. Rock Min. Anal. 37 (5), 1–4. https://doi.org/10.15898/j.cnki.11-2131/td.201807250088.

Liu, Z., Zhao, M., Sun, H., Yang, R., Chen, B.o., Yang, M., Zeng, Q., Zeng, H., 2017. "Old" carbon entering the South China Sea from the carbonate-rich Pearl River Basin: Coupled action of carbonate weathering and aquatic photosynthesis. Appl. Geochem. 78, 96–104. https://doi.org/10.1016/j.apgeochem.2016.12.014.

Liu, Z., Macpherson, G.L., Groves, C., et al. 2018a, Large and active CO2 uptake by coupled carbonate weathering. Earth-Sci. Rev., 182: 42-49.https://doi.org/10.1016/j.earscirev.2018.05.007.

Liu, Y., He, Q., Liu, L., et al. 2018b, Distinguishing the compositions and sources of the chromophoric dissolved organic matter in a typical karst river during the dry season: A case study in Bitan river, Jinfo Mountain. Environ. Sci., 39(6): 2651-2660. https://doi.org/10.13227 /j.hjkx.201711106.

Lu, X., 2018. Analysis of source and component characteristic of Dissolved Organic Matter in Karst Reservoir Water – a Case Study in Wulixia Reservoir of Guangxi Province. Master Thesis. Southwest University, Chongqing, China.

Martínez–Pérez, A.M., Catalá, T.S., Nieto–Cid, M., Otero, J., Álvarez, M., Emelianov, M., Reche, I., Álvarez–Salgado, X.A., Arístegui, J., 2019. Dissolved organic matter (DOM) in the open Mediterranean Sea. II: basin–wide distribution and drivers of fluorescent DOM. Prog. Oceanogr. 170, 93–106. https://doi.org/10.1016/j.pocean.2018.10.019.

Chen, M., Price, R.M., Yamashita, Y., Jaffé, R., 2010. Comparative study of dissolved organic matter from groundwater and surface water in the Florida coastal Everglades using multi-dimensional spectrofluorometry combined with multivariate statistics. Appl. Geochem. 25 (6), 872–880. https://doi.org/10.1016/j.apgeochem.2010.03.005.

Moradi, S., Sawade, E., Aryal, R., W.K. Chow, C., van Leeuwen, J., Drikas, M., Cook, D., Amal, R., 2018. Tracking changes in organic matter during nitrification using fluorescence excitation–emission matrix spectroscopy coupled with parallel factor analysis (FEEM/PARAFAC). J. Environ. Chem. Eng. 6 (1), 1522–1528. https://doi.org/10.1016/j.jece:2018.02.003.

Mudarra, M., Andreo, B., Baker, A., 2011. Characterisation of dissolved organic matter in karst spring waters using intrinsic fluorescence: Relationship with infiltration processes. Sci. Total Environ. 409 (18), 3448–3462. https://doi.org/10.1016/j.scitotenv.2011.05.026.

Murphy, K.R., Ruiz, G.M., Dunsmuir, W.T.M., Waite, T.D., 2006. Optimized parameters for fluorescence- based verification of ballast water exchange by ships. Environ. Sci. Tech. 40 (7), 2357–2362. https://doi.org/10.1021/es051938110.1021/es0519381.s001.

Obernosterer, I., Benner, R., 2004. Competition between biological and photochemical processes in the mineralization of dissolved organic carbon. Limnol. Oceanogr. 49 (1), 117–124. https://doi.org/10.4319/lo.2004.49.1.0117.

Ogawa, H., Amagai, Y., Koike, I., et al., 2001. Production of refractory dissolved organic matter by bacteria. Sci. 292 (5518), 917–920. https://doi.org/10.1126/science.1057627.

Osburn, C.L., Stedmon, C.A., Spencer, R.G.M., Stubbins, A., 2013. Linking optical and chemical properties of dissolved organic matter in natural waters. Limnol. Oceanogr. Bull. 22 (3), 78–82. https://doi.org/10.1002/lob.201322378.

Pain, A. J., Martin, J. B., Young, C. R., et al. 2020, Carbon and phosphorous processing in a carbonate karst aquifer and delivery to coastal ocean. Geochim. Cosmochim. Ac., 269: 484-495.https://doi.org/10.1016/j.gca.2019.10.040.

Passow, U., Carlson, C.A., 2012. The biological pump in a high CO_2 world. Mar. Ecol. Prog. Ser. 470, 249–271. https://doi.org/10.3354/meps09985.

Posth, N.R., Bristow, L.A., Cox, R.P., Habicht, K.S., Danza, F., Tonolla, M., Frigaard, N.-U., Canfield, D.E., 2017. Carbon isotope fractionation by anoxygenic phototrophic

bacteria in euxinic Lake Cadagno. Geobio 15 (6), 798–816. https://doi.org/10.1111/gbi.2017.15.issue-610.1111/gbi.12254.

Pu, J., Li, J., Zhang, T., et al. 2020, Varying thermal structure controls the dynamics of CO2 emissions from a subtropical reservoir, south China. Water Res., 178: 115831. https://doi.org/10.1016/j.watres.2020.115831.

Quiers, M., Batiot-Guilhe, C., Bicalho, C.C., et al., 2014. Characterization of rapid infiltration flows and vulnerability in a karst aquifer using a decomposed fluorescence signal of dissolved organic matter. Environ. Earth Sci. 71, 553–561. https://doi.org/10.1007/s12665-013-2731-2.

Sakellariadou, F., Antivachis, D., 2018. Spectroscopic studies of dissolved organic matter in a heavily modifed Mediterranean and ancient coastal lake. Environ. Earth Sci. 77, 272. https://doi.org/10.1007/s12665-018-7446-y.

Sasaki, H., Miyamura, T., Saitoh, S.-I., Ishizaka, J., 2005. Seasonal variation of absorption by particles and colored dissolved organic matter (CDOM) in Funka Bay, southwestern Hokkaido, Japan. Estuarine. Coastal Shelf Sci. 64 (2-3), 447–458. https://doi.org/10.1016/j.ecss.2005.03.008.

Shabarova, T., Villiger, J., Morenkov, O., Niggemann, J., Dittmar, T., Pernthaler, J., 2014. Bacterial community structure and dissolved organic matter in repeatedly flooded subsurface karst water pools. FEMS Microbiol. Ecol. 89 (1), 111–126. https://doi.org/10.1111/fem.2014.89.issue-110.1111/1574-6941.12339.

Shutova, Y., Baker, A., Bridgeman, J., et al., 2014. Spectroscopic characterization of dissolved organic matter changes in drinking water treatment: from PARAFAC analysis to online monitoring wavelengths. Water Res. 54, 159–169. https://doi.org/10.1016/j.watres.2014.01.053.

Simon, K.S., Pipan, T., Ohno, T., Culver, D.C., 2010. Spatial and temporal patterns in abundance and character of dissolved organic matter in two karst aquifers. Fund. Appl. Limnol. 177 (2), 81–92. https://doi.org/10.1127/1863-9135/2010/0177-0081.

Sun, P., He, S., Yuan, Y., Yu, S., Zhang, C., 2019. Effects of aquatic phototrophs on seasonal hydrochemical, inorganic, and organic carbon variations in a typical karst basin, Southwest China. Environ. Sci. Pollut. Res. 26 (10), 32836–32851. https://doi.org/10.1007/s11356-019-06374-6.

Stedmon, C.A., Markager, S., Bro, R., 2003. Tracing dissolved organic matter in aquatic environments using a new approach to fluorescence spectroscopy. Mar. Chem. 82 (3-4), 239–254. https://doi.org/10.1016/S0304-4203(03)00072-0.

Stedmon, C.A., Markager, S., Bro, R., 2008. Characterizing dissolved organic matter fluorescence with paral-lel factor analysis: a tutorial. Limnol. Oceanogr.: Methods 6 (572–579). https://doi.org/10.4319/lom.2008.6.572.

Song, A., Peng, W., He, R., et al., 2017. Hydrochemistry characteristics in front of the Wulixia reservoir dam associated with feedback from aerobic anoxygenic phototrophic bacteria. Rock Min. Anal. 36 (2), 171–179. https://doi.org/10.15898/j.cnki.11-2131/td.2017.02.11.

Tatár, E., Mihucz, V.G., Zámbó, L., Gasparics, T., Záray, G., 2004. Seasonal changes of fulvic acid, Ca and Mg concentrations of water samples collected above and in the Béke Cave of the Aggtelek karst system (Hungary). Appl. Geochem. 19 (11), 1727–1733. https://doi.org/10.1016/j.apgeochem.2004.03.011.

Xie, X.N., Wang, S.J., Zhou, Y.C., Luo, W.J., 2008. Three-dimensional fluorescence spectral characteristics of dissolved organic carbon in cave drip waters and their responses to environment changes: Four cave systems as an example in Guizhou Province. China. Chin. Sci. Bull. 53 (6), 884–889. https://doi.org/10.1007/s11434-008-0079-x.

Yue, H., Chen, Y., 2008. Study on sediment concentration variation in Lijiang River basin. J. Sediment Resear. 3: 58-63. http://doi.org/10.16239/j .cnki .0468-155x.2008.04.010.

Wang, Y., Li, X., Li, B.H., Shen, Z.Y., Feng, C.H., Chen, Y.X., 2012. Characterization, sources, and potential risk assessment of PAHs in surface sediments from nearshore and farther shore zones of the Yangtze estuary, China. Environ. Sci. Pollut. R. 19 (9), 4148–4158. https://doi.org/10.1007/s11356-012-0952-7.

Wang, Q., 2013. Sediment development and water and soil conservation analysis for Guijiang River basin area within Guilin City. Guangxi Water Res. Hydropower Engin., 3: 56-59. http://doi.org/ 1003-1510(2013)03-0056-04.

Wu, X., Bai, X., 2017, Impact of Climate Change on Lijiang River 's Ecological Environment. J. of Meteorol. Res. Appl., 38(1): 97-101. https://doi.org/1673-8411 (2017) 01-0097-03.

Yang, R., Chen, B., Liu, H., Liu, Z., Yan, H., 2015. Carbon sequestration and decreased CO_2 emission caused by terrestrial aquatic photosynthesis: Insights from diel hydrochemical variations in an epikarst spring and two spring-fed ponds in different seasons. Appl. Geochem. 63, 248–260.

Yang, M., Liu, Z., Sun, H., Yang, R., Chen, B.o., 2016. Organic carbon source tracing and DIC fertilization effect in the Pearl River: Insights from lipid biomarker and geochemical analysis. Appl. Geochem. 73, 132–141.

Yuan, Y., 2016. Impacts of Aquatic Organisms on Hydrochemical Characteristics and Karst Carbon Sink in Lijiang Basin. Master thesis. Southwest University, Chongqing, China.

Zhang, Y., van Dijk, M.A., Liu, M., Zhu, G., Qin, B., 2009. The contribution of phytoplankton degradation to chromophoric dissolved organic matter (CDOM) in eutrophic shallow lakes: Field and experimental evidence. Water Res. 43 (18), 4685–4697. https://doi.org/10.1016/j.watres.2009.07.024.

Zhang, Z., Lian, B., Hou, W., et al., 2011. Chen M X. Bacillus mucilaginous can capture atmospheric CO_2 by carbonic anhydrase. Afr. J. Microbiol. Res. 5, 106–112. http://www.academicjournals.org/ajmr.

Zhang, D., Wang, D., 2016. Wang Xilin, Influence of riparian vegetation on surface runoff and sediment in Li R iver of Guilin City. Science of Soil and Water Conservation. 14 (2):81-86. http//doi.org/ 10.16843 /j.sswc.2016.02.011.

Zhang, T., Li, J., Pu, J., Martin, J.B., Khadka, M.B., Wu, F., Li, L.i., Jiang, F., Huang, S., Yuan, D., 2017. River sequesters atmospheric carbon and limits the CO_2 degassing in karst area, southwest China. Sci. Total Environ. 609, 92–101. https://doi.org/10.1016/j.scitotenv.2017.07.143.

Zhang, T., Li, J., Pu, J., Yuan, D., 2019. Carbon dioxide exchanges and their controlling factors in Guijiang River, SW China. J. Hydrol. 578, 124073. https://doi.org/10.1016/j.jhydrol.2019.124073.

Zhao, H., 2018. C-N coupling process in aquatic ecosystem of Lijiang basin. Master Thesis. Southwest University, Chongqing, China.

Zhao, H., Xiao, Q., Zhang, C., Zhang, Q., Wu, X., Yu, S., Miao, Y., Wang, Q., 2020. Transformation of DIC into POC in a karst river system: evidence from $\delta^{13}C_{DIC}$ and $\delta^{13}C_{POC}$ in Lijiang, Southwest China. Environ. Earth Sci. 79, 295. https://doi.org/10.1007/s12665-020-09039-7.

Zhou, Y., Li, Y., Yao, X., Ding, W., Zhang, Y., Jeppesen, E., Zhang, Y., Podgorski, D.C., Chen, C., Ding, Y.i., Wu, H., Spencer, R.G.M., 2019. Response of chromophoric dissolved organic matter dynamics to tidal oscillations and anthropogenic disturbances in a large subtropical estuary. Sci. Total Environ. 662, 769–778. https://doi.org/10.1016/j.scitotenv.2019.01.220.